Fabrication and field emission properties of vertical, tapered GaN nanowires etched via phosphoric acid

IOP Publishing Nanotechnology
Nanotechnology 33 (2022) 035301 (13pp) https://doi.org/10.1088/1361-6528/ac2981

Fabrication and field emission properties of vertical, tapered GaN nanowires etched via phosphoric acid

Barbara A Kazanowska[1], Keshab R Sapkota[2], Ping Lu[2], A Alec Talin[3], Ezra Bussmann[2], Taisuke Ohta[2], Brendan P Gunning[2], Kevin S Jones[1] and George T Wang[2,*]

[1] University of Florida, Department of Materials Science and Engineering, Gainesville, FL 32611, United States of America
[2] Sandia National Laboratories, Albuquerque, NM 87185, United States of America
[3] Sandia National Laboratories, Livermore, CA 94550, United States of America

E-mail: gtwang@sandia.gov

Received 6 July 2021, revised 14 September 2021
Accepted for publication 21 September 2021
Published 27 October 2021

Abstract

The controlled fabrication of vertical, tapered, and high-aspect ratio GaN nanowires via a two-step top-down process consisting of an inductively coupled plasma reactive ion etch followed by a hot, 85% H_3PO_4 crystallographic wet etch is explored. The vertical nanowires are oriented in the [0001] direction and are bound by sidewalls comprising of $\{33\bar{6}2\}$ semipolar planes which are at a 12° angle from the [0001] axis. High temperature H_3PO_4 etching between 60 °C and 95 °C result in smooth semipolar faceting with no visible micro-faceting, whereas a 50 °C etch reveals a micro-faceted etch evolution. High-angle annular dark-field scanning transmission electron microscopy imaging confirms nanowire tip dimensions down to 8–12 nanometers. The activation energy associated with the etch process is 0.90 ± 0.09 eV, which is consistent with a reaction-rate limited dissolution process. The exposure of the $\{33\bar{6}2\}$ type planes is consistent with etching barrier index calculations. The field emission properties of the nanowires were investigated via a nanoprobe in a scanning electron microscope as well as by a vacuum field emission electron microscope. The measurements show a gap size dependent turn-on voltage, with a maximum current of 33 nA and turn-on field of 1.92 V nm^{-1} for a 50 nm gap, and uniform emission across the array.

Supplementary material for this article is available online

Keywords: GaN, nanowire, nanofabrication, etching, H_3PO_4, field emission

(Some figures may appear in colour only in the online journal)

1. Introduction

Gallium Nitride (GaN) is a wide bandgap semiconductor used widely in electronic and optoelectronics, such as lasers and light emitting diodes, high electron mobility transistors, RF devices, and power electronics [1–3]. There is a growing interest in using GaN for novel nanoelectronic device structures. For example, GaN-based nanostructures have broad potential applications in piezoelectronics [4, 5], biocompatible devices [6, 7], solar energy harvesting [8], sensors [9], and field emission [10–12]. Many of these applications rely on fabricating GaN into nanowires as this provides an option for vertical device morphologies. In the realm of optoelectronics and photonics, GaN-based nanowires allow access to non-polar and semipolar crystal planes and have high emitting surface area which could lead to performance improvements in lasers and LEDs [11, 13–15]. To fully harness the potential of the GaN vertical nanostructures, novel approaches are

* Author to whom any correspondence should be addressed.

necessary to fabricate nanostructures to expose various crystallographic facets and control the final 3D shape.

GaN nanowires are commonly realized by bottom-up growth, which has advantages such as low-strain growth, *in situ* core–shell growth, high alloy incorporation [16], and low dislocation densities [17, 18]. However, GaN nanowires fabricated via top-down approaches obviate issues which arise in bottom-up nanowire growth, such as unknown dopant concentration, limited growth regimes, non-uniform growth rates across nanowires, high impurity levels, and a greater number of point-defects [19]. Top-down nanowire fabrication using a lithographic patterning technique followed by plasma etching enables the formation of ordered, periodic arrays with independent control over the height, width, and pitch of the desired nanostructures, and allows for tailored cross-sectional shape control. However, plasma etching alone leaves damaged, tapered, and rough sidewalls [20–24]. The plasma damage on GaN nanowire surfaces causes many issues, namely the promotion of surface recombination, which in turn decreases the near-band-edge photoluminescence by half [25], the creation of trapping potentials for carriers [26], introduction of lattice defects and N vacancies which are shown to be electronically active [27–29], additional carrier depletion [30], and lowering Schottky barrier heights for gate metals in field effect transistors [22, 25, 31–34]. Additionally, for top-down processes, the final dimension of the tip is limited by the lithography process.

To address this issue, steps have been taken to mitigate dry etch damage and to control the shape by introducing a wet chemical etch after the dry etching step. Anisotropic wet etching is commonly used for silicon MEMs devices where crystallographic anisotropy is the key to produce designed geometric structures with atomically smooth facets and a highly controlled final tip diameter. Utilizing a crystallographic wet etch, a two-step dry plus KOH-based wet top-down etch process has been developed to etch high quality, smooth, vertical GaN nanostructures with non-polar sidewall facets [35–40]. This approach has previously been used to demonstrate single mode nanowire lasers, nano LEDs, GaN-based field emission devices, and to showcase novel optical control of polarization and emission of nanoscale lasers [10, 35, 37, 38, 41–44]. Although anisotropic KOH etching of GaN is a promising technique, a major disadvantage of KOH processing is potassium ion (K^+) contamination in dielectrics which result in gate leakage [45–47].

While this KOH-based crystallographic etching has been successfully used to create GaN nanowire-based devices with smooth, vertical sidewalls and flat tips, additional crystallographic etches could expand the scope of possible nanostructure shapes and exposed crystal facets. In particular, the controlled fabrication of GaN nanowires with sharp tips could have applications in scanning probe microscopy or field emission devices. Additionally, there is a growing motivation in the fabrication of gated devices which steps away from KOH-based etching processes due the previously mentioned K^+ contamination, particularly in complementary metal-oxide-semiconductors processes. Here we show a new two-step top-down approach using a crystallographic hot phosphoric acid (H_3PO_4) wet etch to realize tapered, vertical GaN nanowires with sharp tips and semipolar facets which circumvent the use of KOH-based etchants. We present the evolution of the etch process and field emission measurements of the single nanowires and an array of nanowires, which show excellent turn-on uniformity.

2. Experimental

2.1. Nanowire fabrication and characterization methods

Epitaxial single crystal GaN was grown by metalorganic chemical vapor deposition in a Taiyo Nippon Sanso SR4000HT reactor on 2 inch *c*-sapphire substrates, with n-type doping using Si at a concentration of $3e18/cm^3$. Arrays of variable diameter dots (300 nm to 1 μm in diameter) were patterned in a spin-coated polymethyl methacrylate layer on GaN followed by electron beam lithography (EBL). EBL was carried out by both the nanometer pattern generation system (NPGS) attached to an FEI Nova NanoSEM 450 scanning electron microscope (SEM) and a JEOL JBX-6300FS system. NPGS was used to pattern 300 nm dots with a 2 μm pitch and 1 μm dots with an 8 μm pitch to be used for initial etching studies. The JEOL was used to pattern dots with a 1.3 μm diameter with a 20 μm pitch to be used in field emission studies. After pattern development, a metal mask consisting of Ti (5 nm)/Ni (100–150 nm) was deposited and soaked in acetone for the lift-off. In addition to EBL patterning, other samples were patterned using a layer of self-assembled SiO_2 microspheres with a 1 μm diameter as a semi-periodic, large area, plasma etch mask [35, 37, 41, 42, 44, 48]. An inductively coupled plasma reactive ion etch (ICP-RIE) of $Cl_2/Ar/BCl_3$ chemistry at a chamber and chuck temperature of 65 °C was used to etch the initial nanowire structures to a depth of 1–1.4 μm. The remaining metal mask was removed in piranha etch for 10 min to fully clean the sample surface, which was followed by a two-minute buffered oxide etch (BOE) soak to remove any native oxide. Immediately after the BOE soak, the nanowire samples were all etched in ~150 ml of hot, 85% H_3PO_4 at temperatures between 50 °C and 95 °C for varying times, and then subsequently imaged in a FEI Nova NanoSEM 450 SEM. GaN nanowires were scraped directly from the substrate with a razor blade and dispersed randomly on to carbon film supported on a Cu TEM grid by rubbing the blade tip against the carbon film. A FEI Titan^{TM} G2 80–200 scanning transmission electron microscope (STEM) with a Cs probe corrector operated at 200 kV was used to image the nanowires. STEM images were recorded by using a high-angle annular dark-field (HAADF) detector. The GaN nanowires were tilted to either a $[10\bar{1}0]$ or $[11\bar{2}0]$ zone axis for high-resolution imaging of the tips.

2.2. Field emission methods

Field emission measurements of individual GaN nanowires fabricated by this approach were conducted in an SEM

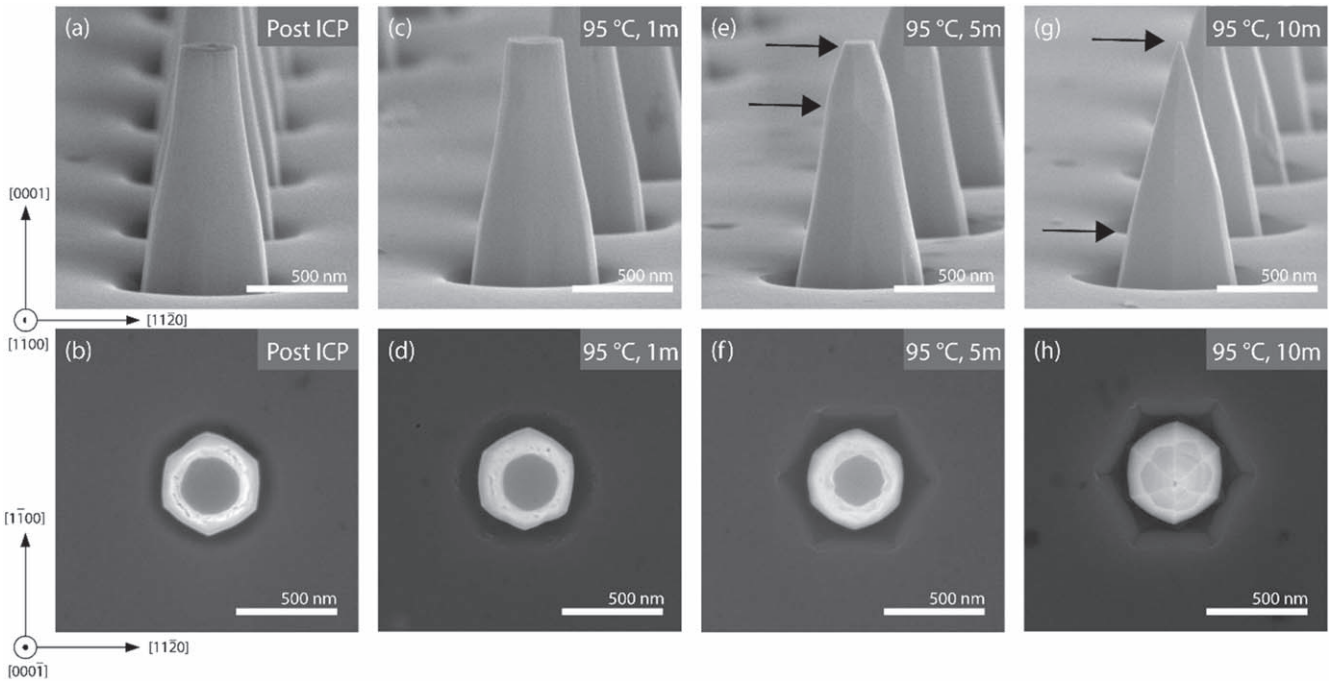

Figure 1. Side and top down SEM images of 300 nm diameter GaN nanowires etched in 95 °C H_3PO_4 at (a), (b) 0 min, (c), (d) 1 min, (e), (f) 5 min, and (g), (h) 10 min.

equipped with a nanomanipulator probe. For both single nanowire and array field emission studies, the GaN nanowires were ∼3 μm in height patterned with a 20 μm pitch and were not etched down to the sapphire substrate, leaving a ∼300 nm n-type GaN base layer connecting the nanowire array. The SEM system used for field emission studies has been described in detail elsewhere [49], and similar systems have been used extensively in the past to characterize the field emission characteristics of various nanostructures [50]. In the present case, a Au coated W nanotip with a radius of curvature of 1 μm as the anode was used. The base pressure during the FE measurements was between 5×10^{-7} and 1×10^{-6} Torr. The nanowire sample was mounted on a specimen holder using vacuum compatible Ag paint which also served to make an Ohmic contact to the substrate. The field emission current was collected as a function of applied voltage using a PC-controlled Keithley 237 source-measure unit.

To visualize and compare qualitative field emission characteristics across arrays of nanowires, field emission images of nanowire arrays were obtained using a field emission microscope (FEM) [51]. Here, we implemented a FEM utilizing electron optics of a commercial ultrahigh vacuum ($<10^{-9}$ Torr) low-energy/photoemission electron microscope (LEEM/PEEM, *Elmitec GmBH*) [52]. The field emission current was extracted by positioning a sample, biased at −15 keV, at adjustable millimeter-scale distances from a grounded cathode objective lens. It is not possible to measure the sample-objective distance with an accuracy greater than ∼0.1 mm, which yields ∼10% uncertainty in the applied electric field. The image is acquired by a digital camera, and the spatial resolution of the apparatus is around 10 nm (limited by aberration) [53].

3. Results and discussion

3.1. GaN nanowires etched in H_3PO_4

Figure 1 shows side- and top-down view SEM images of nanowires prepared by plasma-etching followed by H_3PO_4 etching at 95 °C for increasing times. Figures 1(a) and (b) show the nanowires after the remaining metal mask was stripped but prior to H_3PO_4. This slight faceting at the base of the nanowires from ICP-RIE etching of GaN in Cl_2 chemistry is well documented in the literature [54–56], and these facets here are oriented in the $\langle 11\bar{2}l \rangle$ *a*-type direction. There is also an apparent trench at the base of the dry-etched nanowires which is thought to appear due to the Ti/Ni mask erosion at extended high-bias plasma etching [32, 57, 58]. The observed tip diameter was 290 ± 10 nm and the nanowires were ∼950 nm in height. Approximately 20–30 nanowires were measured here and for each successive temperature and time point, where the nanowire height and diameter are average values with the error equal to one standard deviation. Figures 1(c)–(h) show the etch progression of the GaN nanowires in 95 °C H_3PO_4 at 1, 5, and 10 min from the side and top down views. Note that the figures do not track the same nanowire since different samples were used for each etch point. However, many tips were studied at each time to verify the consistency of the results. From this etch time progression, a distinct group of semipolar facets appear around the tip perimeter. Particularly in figures 1(e) and (g) as designated by the arrows, we observe the appearance of a semipolar facet at the tip of the nanowire, and with time, the facet extends further down the length of the nanowire. Top down views confirm that the semipolar facet planes are of the $\{11\bar{2}l\}$ *a*-type orientation with the nanowire tip cross section

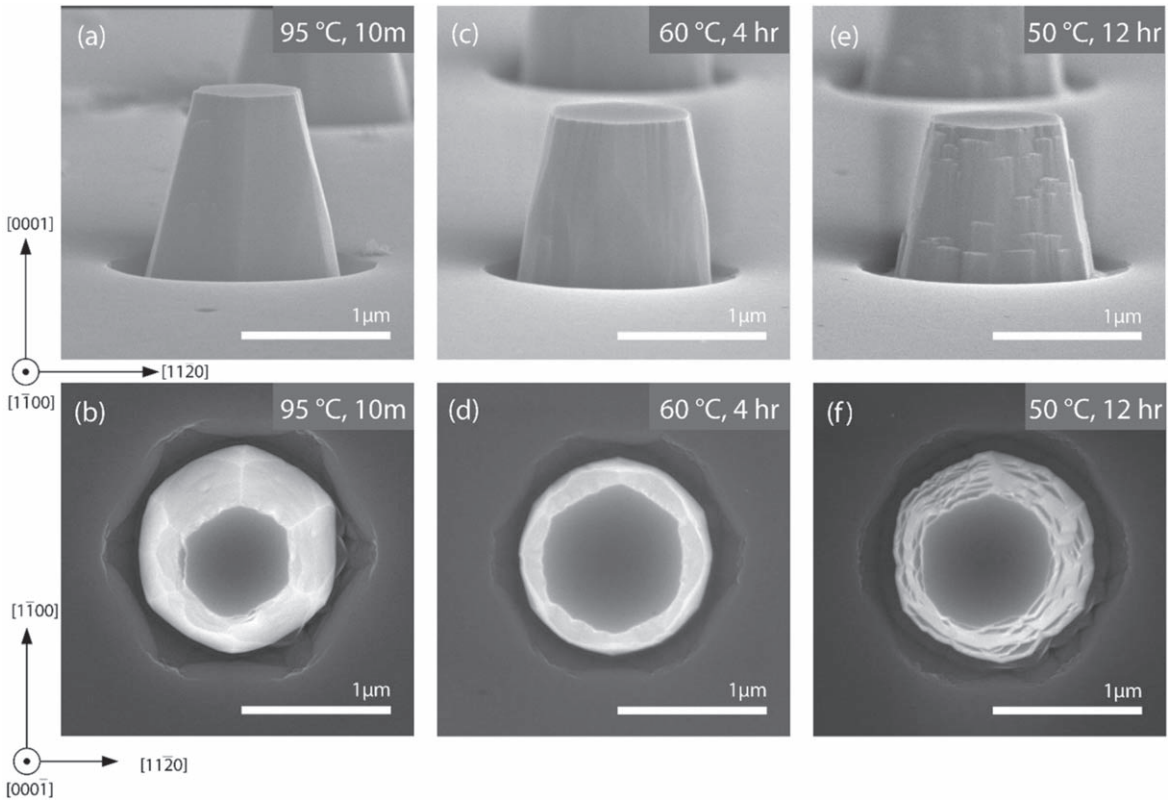

Figure 2. A comparison of the etch evolution and semipolar facet morphology of 1 μm GaN nanowires etched in H_3PO_4 at (a), (b) 95 °C for 10 min, (c), (d) 60 °C for 4 h, and (e), (f) 50 °C for 12 h.

eventually transitioning to be hexagonal in shape before etching to a fine point. From SEM analysis of the as-etched pyramidal nanowires, the estimated angle of the top semipolar facet was 12° from the [0001] *c*-direction, which was consistent across different nanowires and at different etch times. Previously, it has been reported that H_3PO_4 etches N-face (000$\bar{1}$) GaN into dodecagonal pyramids [59–62] and etches hexagonal pits at defect sites in Ga-face (0001) GaN [61, 63–66]. Thus, the H_3PO_4 etch for GaN can be considered crystallographic in nature, much like the KOH-based etch, but with semipolar rather than nonpolar planes being exposed.

Figure 2 shows a temperature dependent etch study of GaN nano-pyramidal nanowires in 85% H_3PO_4 at three different temperatures. In this figure, larger diameter nanowires were used to better illustrate the etch evolution. Similarly to figure 1, figures 2(a) and (b) show a nanowire etched in 95 °C H_3PO_4 where six smooth, semipolar facets are visible. As the temperature of the etchant is decreased to 60 °C, a slight roughening of the semipolar facets is observed in the form of vertical striations on the etched facets as seen in figures 2(c) and (d). When the H_3PO_4 temperature is dropped to 50 °C, pronounced micro-faceting on the semipolar facets is evident, as seen in figures 2(e) and (f). From the top down view in figure 2(f), small, triangular ridges are observed. We posit that the etch appears to begin at the nanowire tip edge, where a nucleation site for the etch is located, and after the initial atoms are removed, the etched layer moves down the semipolar facet of the nanowire atomic layer by layer. At the lower 50 °C etch, the ledges become wider and more visible and the etch progresses via appearance and disappearance of these micro-facets on the nanowire sidewalls.

To further investigate the formation and evolution of the micro-facets observed in figures 2(e) and (f), the etch progression at 50 °C as a function of time for a 300 nm nanowire is presented in figure 3. Similar to the etching behavior of GaN nanowires in KOH, the micro-facets primarily appear to be bound *m*-type semipolar planes on the sides. The top planes of the micro-facets appear to be bound by either a (0001) *c*-plane, or a semipolar plane nearly parallel to the *c*-plane. Leung *et al* noted that the etch of GaN in KOH progressed via the appearance and disappearance of semipolar facets at the convex edges of the nanowire [67], and therefore a similar type of etch progression may be occurring in H_3PO_4, but leading to the appearance of stable semipolar facets rather than the vertical non-polar facets observed in KOH-based etching. A similar tapered geometry is exposed via a digital etching process developed by Shih *et al* where a 1:1 mixture of H_2SO_4:H_2O yields GaN nano-pyramids [12]. Much like what was observed in figure 1, figure 3 shows the cross section at the tip shifts from roughly circular to hexagonal in nature by way of appearing and disappearing triangular *m*-type oriented micro-facets, and at 50 °C, these micro-facets are larger and more apparent compared to higher temperature etching. While the etch is qualitatively different from that at temperatures greater than 60 °C in terms of the observed microfaceting, the end result of a tapered nanowire bound by the same semipolar facets offset by 12 degrees from the (0001) *c*-direction is the same at all temperatures. Sangwal

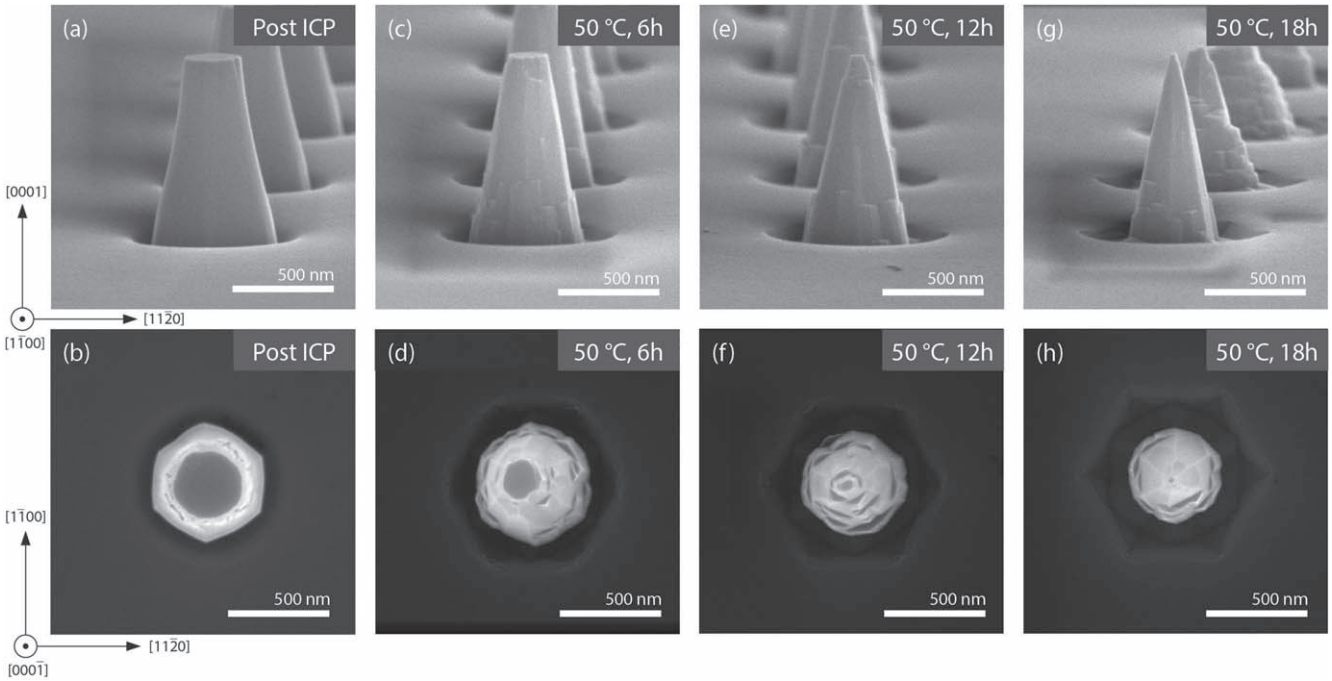

Figure 3. Side and top down view of 300 nm GaN nanowires etched in 50 °C H_3PO_4 at (a), (b) 0 min, (c), (d) 6 h, (e), (f) 12 h, and (g), (h) 18 h.

et al discussed that the effect of viscosity of H_3PO_4 and H_2SO_4 plays an important role in the etching of MgO crystals, where the viscosity of an etchant is used to determine if the dissolution process is diffusion limited [68]. In the case of ~85% H_3PO_4, its viscosity abruptly changes between 50 °C and 60 °C. Since the viscosity change occurs over the same temperature range that the change from smooth to micro-faceted etching occurs, the acid viscosity may play a role in the formation of micro-facets.

STEM was performed to obtain higher resolution views of the etched nanowires and identify the exposed planes. Figure 4 displays a HAADF-STEM image of a singular pyramidal nanowire after etching in 95 °C H_3PO_4 for 55 min. The starting diameter of this nanowire was ~1 μm, and therefore the time required to etch to an ultrasharp tip was greater than that in figure 1. The beam is aligned along the *m* direction [10$\bar{1}$0], and the image shows intersection of two of the semipolar planes which bound the pyramidal nanowire. The top left inset in figure 4 demonstrates the capability of the H_3PO_4 etch to taper a GaN nanowire down to a few nanometers in diameter at the tip, with figure 4 showing a 12 nm diameter. The smallest tip diameter observed from a sampling of nanowires on this sample was 8 nm, and can be seen in figure S1 (available online at stacks.iop.org/NANO/33/035301/mmedia), however we were not able to image this nanowire on the zone axis resulting in an unclear fast Fourier transform (FFT) of the diffraction pattern. With further fine tuning of the etch process, it is possible that even finer tip dimensions might be realized. Top down fabrication of hexagonal GaN nanowires with diameters less than 10 nm has not been previously reported to our knowledge, with the smallest

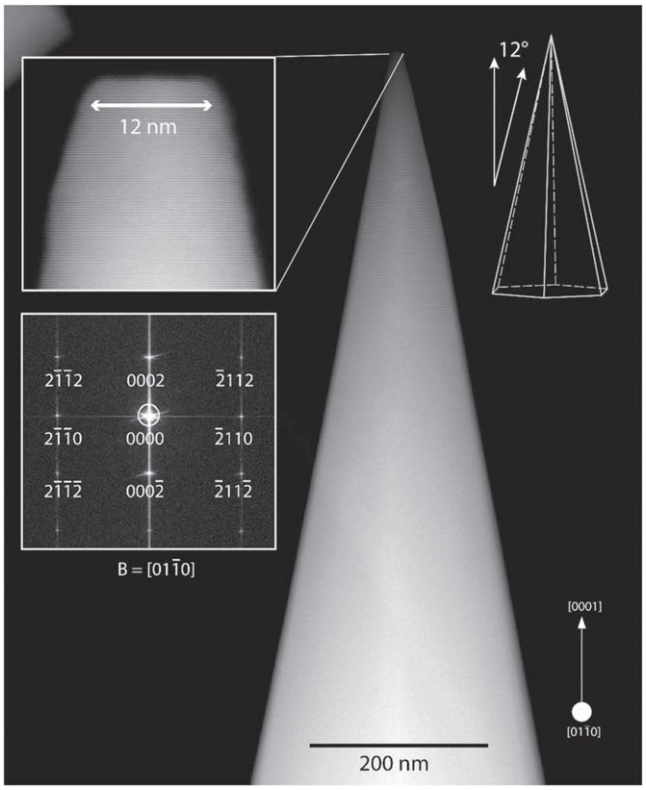

Figure 4. HAADF-STEM of a GaN nanowire etched in 95 °C H_3PO_4 for 55 min. The top left inset shows the measured tip diameter (12 nm). The bottom left inset is the indexed diffraction pattern indicating the beam direction is parallel to the [10$\bar{1}$0], *m*-direction zone axis. A 3D model of the nanowire pyramid is included as the top right inset. The electron beam is oriented down the intersection of two *a*-type semipolar facets.

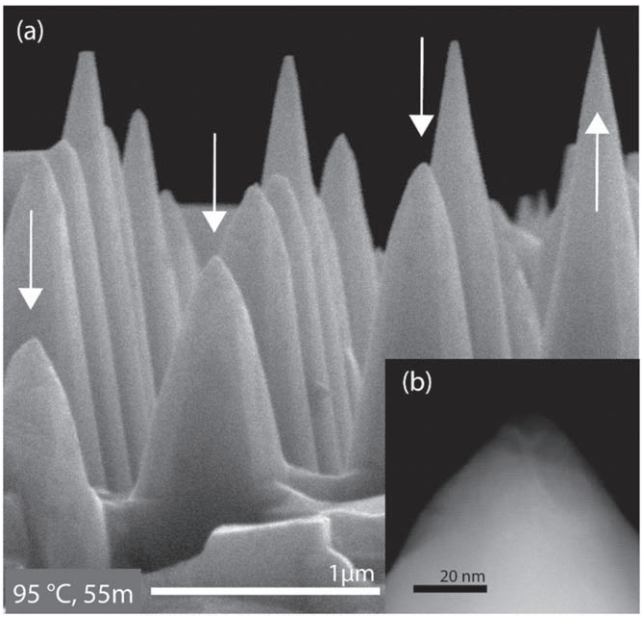

Figure 5. (a) GaN nanowires over-etched after 55 min at 95 °C in H_3PO_4, (b) HAADF-STEM inset of an over-etched nanowire tip.

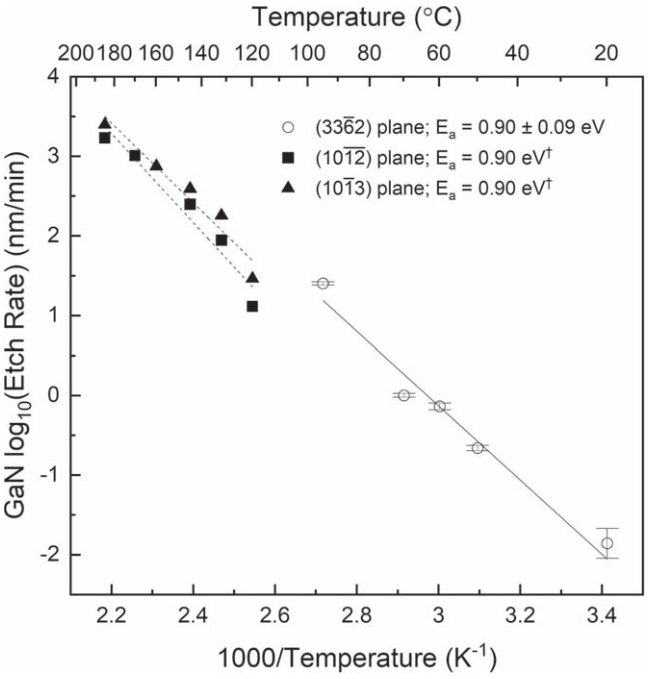

Figure 6. Arrhenius plot of etch rates for 300 nm GaN nanowires in 85% H_3PO_4. Hollow circles indicate etch rates from this work, measured laterally at the tip of the nanowire and corrected by a cosine of 12° multiplication factor to account for the semipolar facet. †literature data from D.A. Stocker *et al* [63].

reported tip diameter of 15 nm [12]. Such tapered, ultrasharp nanowires could be of interest for applications such as field emitters or scanning probes. The bottom inset in figure 4 is a fast FFT of the HAADF-STEM image. After indexing the FFT pattern, the Miller indices of the semipolar facets were found to be in the {33$\bar{6}$2} family of high-index planes. A detailed figure elaborating on the method used to index the diffraction pattern is presented in figure S2.

Extended etch times were also studied to determine the over-etch progression of the GaN nanowires. Figure 5(a) shows GaN nanowires etched 95 °C GaN for 55 min, starting with an initial diameter of 1 μm. Wires of different heights are observed, indicating that the wires become shorter with etching after the tip (0001) facet is completely etched away. This sample was patterned using a SiO_2 microsphere semi-periodic mask, and the starting base diameter ($\sim$1 μm) of the nanowires post-ICP etch varied more than the EBL-patterned sample. Figure S3 shows the starting point for these nanowires post ICP-RIE and prior to wet etching. Figure 5(b) is a HAADF-STEM image of an over-etched nanowire tip indicating the tip planes exposed during over etch are lower in angle, and thus the tip is blunted. No consistent planes appear to be observed in the over-etched nanowires, possibly suggesting that the top (0001) *c*-plane facet plays a key role in the exposure of the {33$\bar{6}$2} semipolar planes during the etch. Similar etching has been seen in palladium [69] and gold [70] nanocrystals and silicon [71] hillock geometries where the apexes of the structures etch first due to the lower coordination and higher reactivity of atoms at the tip. For further process control, a mask protecting the nanowire tip may be a method to prevent over-etching.

Figure 6 shows an Arrhenius plot of etch rates in 85% H_3PO_4 perpendicular to the {33$\bar{6}$2} plane determined from the temperature series of our GaN nanowires. The etch rates at five temperatures were measured perpendicular to the {11$\bar{2}$0} *a*-plane and multiplied by the cosine of 12° since the {33$\bar{6}$2} facet intersects the *a*-plane at a 12 degree angle. This converts the etch rate measured in the 11$\bar{2}$0 direction to that of 33$\bar{6}$2 >. The extracted activation energy is 0.90 ± 0.09 eV. This value is in line with activation energies from previously reported H_3PO_4 etch studies of GaN of 0.9 [63], and indicates that the etch is reaction-rate limited [72–74]. The data is plotted against GaN in H_3PO_4 data from the literature, and the activation energy of the nanowire etch is in line with the previous reports.

3.2. Etch mechanism and the etch barrier index of GaN in H_3PO_4

The etching of GaN in KOH and tetramethylammonium hydroxide (TMAH) has been previously reported to progress via formation of surface oxides and then the subsequent dissolution of the oxide in solution. The mechanism for the etch as suggested by Li *et al* here in equation (1), assumes the oxidation of the gallium (Ga) atoms via hydroxide (OH^-) molecules attacking and breaking the Ga–N bonds, freeing the Ga atom to oxidize into Ga_2O_3 which is then dissolved [75]. Conversely, H_3PO_4 dissociates within solution into protons (H^+) and dihydrogen phosphate ($H_2PO_4^-$), hydrogen phosphate ($H_1PO_4^{2-}$), and phosphate groups (PO_4^{3+}) and thus does not result in OH^- molecules to etch the GaN surface via oxide formation and dissolution like the KOH/TMAH etch. In aqueous solutions, phosphoric acid dissociates into some combination of the three anions. Using the solution pH and subsequent equilibrium constants, it is possible to determine

which anionic species is most concentrated within the solution. At a concentration of 85%, the pH of H_3PO_4 is near 0, which indicates that the main anionic species in solution is $H_2PO_4^-$. Reiner *et al* postulate a three-step mechanism where the $H_2PO_4^-$ anionic species attack the Ga atom, which is followed by a bond rearrangement, and then the Ga atom dissolves into solution as a metal-phosphate complex $GaH_2PO_4^{2+}$ as written in equation (2) [66]. The nitrogen atoms are attacked by H^+ which forms NH_3, which is subsequently trapped in the acid in the form of $NH_4(H_2PO_4)$. It is suggested that the $GaH_2PO_4^{2+}$ precipitates in the solution in the form of $GaPO_4$ [76], however there was no precipitate noticed in this work due to the large amount H_3PO_4 used. The difference between an OH^- based etch versus a H^+ based etch is that while the KOH acts similarly to an etch catalyst, the $H_2PO_4^-$ is a reacting species, however, both proposed mechanisms suggest the etch progresses primary via reaction with the Ga atoms

$$2GaN + 3H_2O \overset{KOH}{\rightarrow} Ga_2O_3 + 2NH_3, \quad (1)$$

$$GaN + 2H_2PO_4^- + 4H^+ \overset{yields}{\rightarrow} GaH_2PO_4^{2+} + NH_4(H_2PO_4). \quad (2)$$

Following Reiner's work on the etching of pits in GaN in H_3PO_4, the differences in sidewall angle of our structures can only occur if the etch rate in the lateral direction changes. This vertical versus lateral etch rate ratio has been thoroughly noted in literature for the etching of etch pits [77] and extended to the etching of nanopyramids [60, 78]. When GaN nanowires are etched in KOH, the result is vertical nanowires with atomically smooth sidewalls. It appears that the ratio of the vertical etch rate to the lateral etch rate is so great that there is no opportunity for the nanowire sidewall to be tapered. When looking at the tapered nanowires etched in H_3PO_4 presented in this work, it follows that the ratio of vertical etch rate to that of the lateral etch rate is slightly less than that in KOH. Similarly, when analyzing etch pits formed in GaN via KOH and H_3PO_4 etching, the etch pits formed via H_3PO_4 had a smaller vertical to lateral etch rate ratio, therefore making the H_3PO_4 etch pits shallower than that of those etched in KOH. An accepted explanation for this stems from the difference in size between OH^- and the various H_3PO_4 species, where the smaller hydrodynamic radius of the OH^- anion allows the etch byproducts to diffuse away from the etched surface much more rapidly and therefore allows for greater vertical etch rates, resulting in steeper sidewalls bounding the etch pits, and subsequently, nanowires [66]. To examine why the semipolar plane exposed during the H_3PO_4 etch was $\{33\bar{6}2\}$, calculations of the etch plane potentials was performed.

A quantitative measure of the etching potential between different GaN crystallographic planes has previously been introduced by Lai *et al* in the form of a calculated etching barrier index (EBI) for the etching of GaN in KOH [79]. The EBI is defined as the planar atomic density of the crystallographic plane multiplied by the number of dangling bonds per nitrogen atom in that plane, and gives a value to the etching ability of a plane where the higher the EBI value, the more difficult it is to etch a particular plane. Based on Li's etch mechanism of GaN in KOH, a lower planar density results in fewer nitrogen dangling bonds, and therefore, less steric hinderance for the OH^- ions to attack the Ga-N bonds and bond with the Ga. The negative charge on nitrogen atoms repels the OH^- ion, therefore, a higher planar density with more nitrogen dangling bonds per unit area is more chemically stable. Since the H_3PO_4 etch mechanism also progresses via a negative species attacking the Ga atom, we propose using the same EBI framework to understand this etch progression. It is important to note that the EBI does not take into consideration any calculated surface energies or surface reconstructions, and thus represents a first approach to understanding the etch process rather than a complete theory.

To better understand the etch progression observed in our nanowires, the EBI was calculated for various polar, semipolar, and nonpolar planes of GaN. The planes which were chosen are the major low index planes from the GaN wurtzite crystal structure, and further higher index planes located along the great circle which runs from the (0001) center to the $(11\bar{2}0)$ edge on a (0001) stereographic projection for a hexagonal GaN crystal. The angle from lateral, θ, is defined as the angle between a semipolar or nonpolar plane and the basal (0001) *c*-plane. The planar density, ρ_{planar}, was calculated using the position-duplication-number method [80] and the number of nitrogen dangling bonds, n_N, was determined manually. Note that for certain planes, there is a fractional number of nitrogen dangling bonds. This is due to the asymmetric nature of the atomic stacking within the GaN crystal, where the positioning of the plane in the crystal structure gives the number of dangling bonds to be 1, 2, or even a fraction value of 1.3 or 1.5 [81]. Therefore, to calculate n_N, incremental slices for each plane spanning the d-spacing were taken and the number of nitrogen dangling bonds was calculated as seen in figure S4. A more thorough explanation of the methodology is presented in the supplementary information. The average value of the nitrogen dangling bonds was determined across the d-spacing to account for the variation in where the etch plane is at any given moment during the etch. Table 1 show the calculated EBIs of the major low index planes and *a*-type planes in decreasing order. The EBI calculations show that the $\{33\bar{6}2\}$ plane, which is the experimentally observed facet exposed by the H_3PO_4 etch, has the lowest EBI within the *a*-type $\{11\bar{2}l\}$ planes considered. Therefore, barring any unusual surface energies or surface reconstructions, it can be presumed that a low EBI corresponds to the exposure of a plane during the etch.

3.3. Field emission of GaN nanowires and nanowire arrays

The capability to fabricate GaN nanowires with sharp tips via a top-down approach is attractive for field emission applications such as on-chip electron sources or vacuum nanoelectronic devices [10–12]. GaN in particular has many superior properties which make it an attractive choice for field emission, namely low electron affinity, high thermal and chemical stability, radiation hardness, and a high breakdown field [1, 10]. To explore the potential of the sharp GaN nanowires

Table 1. Angle from lateral, planar density, number of N dangling bonds, and the etching barrier index (EBI) for various GaN prism planes in order of decreasing EBI.

Prism plane	Miller index	Angle from lateral	P_{planar} (atom/Å^2)	n_{N} (1/atom)	EBI (1/Å^2)
$+c$	(0001)	0	0.1116	3	0.3348
m	$\{10\bar{1}0\}$	90	0.1187	1.27	0.1511
a	$\{11\bar{2}0\}$	90	0.137	1	0.137
$-c$	$\{000\bar{1}\}$	0	0.1116	1	0.1116
s2	$\{11\bar{2}2\}$	58.4	0.0584	1.27	0.0743
s5	$\{10\bar{1}1\}$	62	0.0524	1.27	0.0667
	$\{11\bar{2}4\}$	39.1	0.0433	1.45	0.063
r/s4	$\{10\bar{1}2\}$	48.4	0.0407	1.27	0.0518
	$\{11\bar{2}6\}$	28.5	0.0327	1.41	0.0461
	$\{33\bar{6}1\}$	83.6	0.0454	1	0.0454
	$\{33\bar{6}3\}$	72.4	0.0437	1	0.0437
s6	$\{20\bar{2}1\}$	75	0.0287	1.32	0.0378
s3	$\{11\bar{2}1\}$	72.9	0.0328	1.14	0.0373
	$\{44\bar{8}1\}$	85.1	0.0342	1	0.0342
s1	$\{11\bar{2}3\}$	47.3	0.0252	1.32	0.0332
	$\{33\bar{6}2\}$	**78.4**	**0.0224**	**1**	**0.0224**

described in this regard, their field emission properties were individually measured using a nanomanipulator probe mounted in an SEM. This approach has two important advantages: first, the gap separating the emitting nanowire tip (cathode) from the collector probe (anode) can be arbitrarily set and measured accurately and second, the shape and other details of the emitter can be imaged with high resolution. To make it easier to precisely set the cathode-anode gap and to simplify the system electrostatics, the nanoprobe tip was intentionally flattened by pressing it against the substrate (in an area without nanostructures). Field emission current versus voltage (I–V) characteristics collected in vacuum at four different cathode-anode gaps ranging from 50 to 360 nm are displayed in figure 7(a). The I–V data represent initial sweeps with no prior conditioning of the nanowires was performed. An SEM image showing the GaN nanowire tip measured, with a tip width of 20 nm and the probe are shown as an inset. The turn-on voltage for field emission is shown to be increasing with gap size as would be expected for field emission and not leakage or background current through the circuit.

The same data are displayed on a Fowler–Nordheim (FN) plot in figure 7(b). The plot shows a nonlinearity which can be sectioned into three, discrete regions where two regions of linear behavior are separated by a region of a lower slope. FN plots with similar, discrete regions have been previously noted in literature [82–88]. Similar field emission characteristics reports for Si and Ge emitters were explained by a charge depletion zone at the tip, resulting in FN emission at lower fields, followed by current saturation and finally rapid current rise due to secondary charge effects with increasing voltage [89]. Given the large surface to volume ratio and largely un-passivated surface, it is possible that the nanowires in the present case are also depleted, as previously observed for GaN nanowires [90–92]. Reports by Baskin *et al* theoretically analyze field emission behaviors of n-type semiconductors based on the field emission from the conducting band, and further analysis of this work by Al-Tabbakh *et al* concludes that the conducting band current saturation and a dominance of the valence band current at high fields results in nonlinear Fowler–Nordheim characteristics similar to those observed here [86, 93]. We note that field emission from semiconductors is not fully understood or explored, and a more thorough and detailed understanding of the field emission behaviors is outside the scope of this work and will require further investigation. Figure 7(c) displays the turn-on field plotted against gap size for each of the four gap sizes studied in figures 7(a) and (b). The turn-on field here is defined as the voltage required to achieve a current of 0.1 nA, which is roughly 100x the noise floor, divided by the gap size. The observed trend is a decrease in the turn-on field with an increase in gap size, which is expected for our geometry, and has been seen previously in Sim *et al* [94].

For device applications, uniform and reproducible emission characteristics across emitter ensembles are desirable [10]. Since field emission currents are exponentially sensitive to emitter-specific properties such as shape and surface work function, widely-varying field emission characteristics, e.g. turn-on voltage, across the individual emitters within arrays are common and present a key challenge [95–97]. Here, we utilize FEM to visualize and compare properties such as turn-on field, brightness (emission current), and temporal stability for an array of sharp GaN nanowires etched by H_3PO_4 with an average tip diameter of 30 nm $\pm$ 5 nm. The maximum useful electric field is limited by sporadic electrical arc events between the sample mount and the objective lens that interrupt measurements. Similar to typical LEEM/PEEM imaging, spatially resolved images of field emission current density (image brightness) are gathered via a small aperture in the objective lens, though which emission current passes into a series of electromagnetic lenses that magnify and project the field emission current onto a

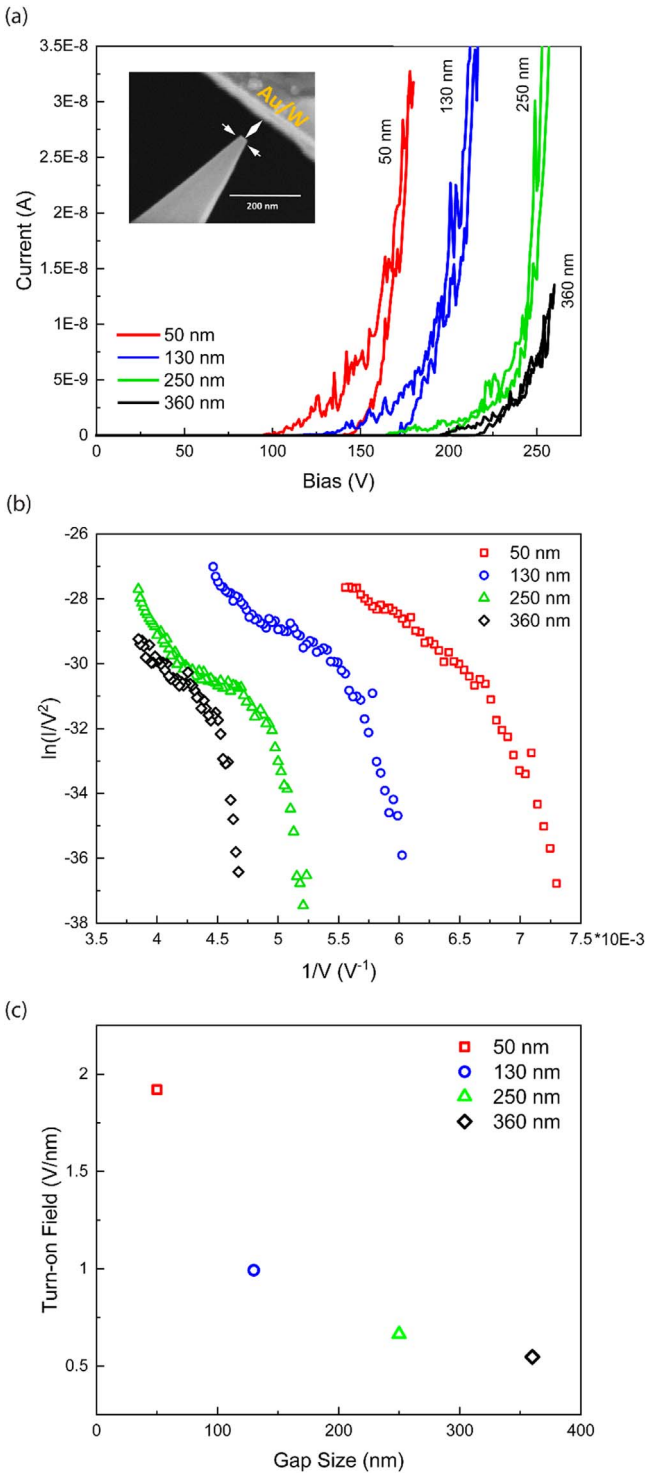

Figure 7. Field emission of GaN nanowires where (a) a 20 nm tip was measured as a function of gap dependence. The inset in (a) depicts the GaN nanowire tip in the vicinity of the Au/W probe tip (b) a Fowler–Norheim plot of the GaN nanowires as a function of gap size, where each curve shows a deviation from linearity at higher applied fields, and (c) the turn-on field in V/nm plotted versus gap size.

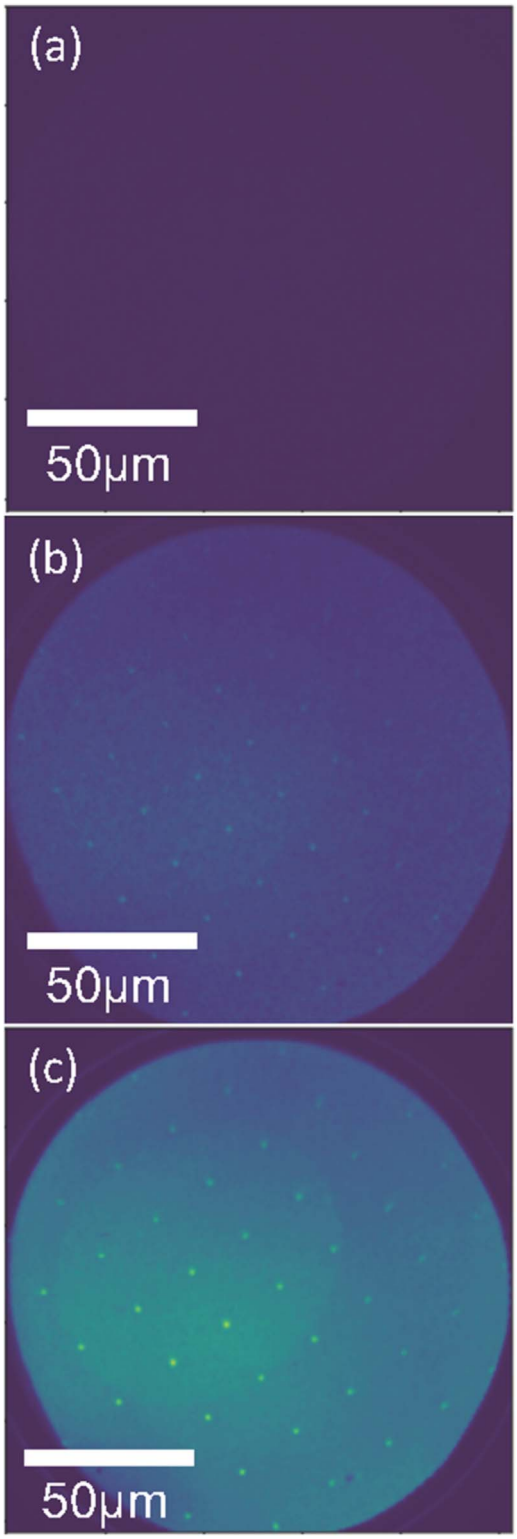

Figure 8. Field emission microscope images versus electric fields: (a) 0.75×10^7 V m^{-1}, (b) 1.2×10^7 V m^{-1}, and (c) 1.5×10^7 V m^{-1} show the homogeneity of current–voltage relationships (brightness *versus* field) across ensembles of emitters. The brighter oval-shaped feature is a spurious defect on the phosphorescent view screen, and the image peripheries are slightly distorted from field inhomogeneity in the electron optics. The field of view for all images is 150 μm in diameter.

microchannel plate that amplifies an image intensity on a phosphorescent screen. Figure 8 shows three FEM images at varying electric fields, where uniform electric fields with

mean values up to 1.5×10^7 V m^{-1} along the sample-objective axis are achieved. We observe that all nanowires turn on with comparable brightness at comparable fields. Qualitatively, the emission homogeneity compares favorably to other types of emitters, e.g. diamond microtips and GaN micro pyramids, in recent literature [96, 97]. A few properties of our nanowires are likely to support this uniform field emission behavior. First, uniform shapes, dictated by strong etch anisotropy and smooth facets (at higher etch temperatures) point to uniform *I–V* characteristics over ensembles of nanowires. Second, in a macroscopic array view where the tip diameter is negligible, the small family of $\{33\bar{6}2\}$ facets represented in equal proportion across all nanowires within the array points to similar electron affinities (and work functions) by mitigating effects of anisotropic, facet-dependent electron affinities which are dominant at nanometer length scales [96]. Third, compared to bottom-up grown nanowires, our top-down fabricated nanowires have very uniform heights of $\sim$3 μm, as well as potentially more uniform doping, further leading to improved field uniformity across the array.

4. Conclusions

In summary, a novel GaN nanowire geometry with sharp tips is presented via a two-step top-down fabrication method. The use of phosphoric acid as the crystallographic, wet chemical etching step results in a hexagonal, tapered GaN nanowire oriented in the [0001] direction bound by the $\{33\bar{6}2\}$ planes. Time and temperature studies of the GaN in phosphoric acid etch reveal a temperature dependence for the etch to progress via appearance and disappearance of microfacets, however, the final structure remains constant across all temperature studies. The activation energy for the GaN in phosphoric acid etch was determined to be 0.9 ± 0.09 eV and is consistent with literature. The EBI was calculated for a range of planes in the hexagonal crystal system and the exposure of the $\{33\bar{6}2\}$ plane is consistent with the EBI prediction. Gap-dependent field emission measurements of the nanowires are presented, and images acquired using a field emission microscope show excellent field emission turn-on and brightness uniformity across an array of nanowires.

Acknowledgments

This work is supported by the Laboratory Directed Research and Development program at Sandia National Laboratories. Sandia National Laboratories is a multi-program laboratory managed and operated by National Technology and Engineering Solutions of Sandia, LLC., a wholly owned subsidiary of Honeywell International, Inc., for the US Department of Energy's National Nuclear Security Administration under contract DE-NA-0003525. This work was performed, in part, at the Center for Integrated Nanotechnologies, a U.S. Department of Energy, Office of Basic Energy Sciences user facility. We acknowledge François Leonard for helpful technical discussions and for a critical reading of the manuscript. This paper describes objective technical results and analysis. Any subjective views or opinions that might be expressed in the paper do not necessarily represent the views of the US Department of Energy or the United States Government.

Data availability statement

All data that support the findings of this study are included within the article (and any supplementary files).

Author contributions

BAK, KSJ, and GTW conceived the concept and design of this study. BAK and KRS fabricated the nanostructures, performed etching experiments, and carried out the characterization and analysis. PL performed HAADF-STEM. AAT performed single nanowire field emission measurements and data analysis. EB and TO performed array field emission measurements and data analysis. BPG carried out the sample growth.

ORCID iDs

Barbara A Kazanowska https://orcid.org/0000-0002-8296-5564
Keshab R Sapkota https://orcid.org/0000-0001-8581-4211
George T Wang https://orcid.org/0000-0001-9007-0173

References

[1] Tsao J Y *et al* 2018 Ultrawide-Bandgap Semiconductors: Research Opportunities and Challenges *Adv. Electron. Mater.* **4** 1600501
[2] Cimalla V, Pezoldt J and Ambacher O 2007 Group III nitride and SiC based MEMS and NEMS: materials properties, technology and applications *J. Phys. D: Appl. Phys.* **40** 6386
[3] Millan J, Godignon P, Perpina X, Perez-Tomas A and Rebollo J 2014 A survey of wide bandgap power semiconductor devices *IEEE Trans. Power Electron.* **29** 2155–63
[4] Wang C-H, Liao W-S, Lin Z-H, Ku N-J, Li Y-C, Chen Y-C, Wang Z-L and Liu C-P 2014 Optimization of the output efficiency of GaN nanowire piezoelectric nanogenerators by tuning the free carrier concentration *Adv. Energy Mater.* **4** 1400392
[5] Gogneau N, Chrétien P, Galopin E, Guilet S, Travers L, Harmand J-C and Houzé F 2014 GaN nanowires for piezoelectric generators *Phys. Status Solidi* **8** 414–9
[6] Jewett S A, Makowski M S, Andrews B, Manfra M J and Ivanisevic A 2012 Gallium nitride is biocompatible and non-toxic before and after functionalization with peptides *Acta Biomater.* **8** 728–33

[7] Zhang M-R, Jiang Q-M, Wang Z-G, Zhang S-H, Hou F and Pan G-B 2017 Three-dimensional gallium nitride nanoflowers supports decorated by gold or silver nanoparticles to fabricate surface-enhanced Raman scattering substrates *Sensors Actuators* B **253** 652–9

[8] Espinet-Gonzalez P *et al* 2019 Radiation tolerant nanowire array solar cells *ACS Nano* **13** 12860–9

[9] Nahhas A M 2020 Review of GaN nanowires based sensors *Am. J. Nanomater.* **8** 32–47

[10] Sapkota K R, Leonard F, Talin A A, Gunning B P, Kazanowska B A, Jones K S and Wang G T 2021 Ultralow voltage GaN vacuum nanodiodes in air *Nano Lett.* **21** 1928–34

[11] Chen F, Ji X and Lau S P 2020 Recent progress in group III-nitride nanostructures: from materials to applications *Mater. Sci. Eng.* R **142** 100578

[12] Shih P C, Rughoobur G, Cheng K, Akinwande A I and Palacios T 2021 Self-align-gated GaN field emitter arrays sharpened by a digital etching process *IEEE Electron Device Lett.* **42** 422–5

[13] Mehari S, Cohen D A, Becerra D L, Zhang H, Weisbuch C, Speck J S, Nakamura S and DenBaars S P 2019 *Semipolar III-Nitride Laser Diodes for Solid-State Lighting* (SPIE)

[14] Li S and Waag A 2012 GaN based nanorods for solid state lighting *J. Appl. Phys.* **111** 071101

[15] Couteau C, Larrue A, Wilhelm C and Soci C 2015 Nanowire lasers *Nanophotonics* **4** 90–107

[16] Li Q and Wang G T 2010 Strain influenced indium composition distribution in GaN/InGaN core–shell nanowires *Appl. Phys. Lett.* **97** 181107

[17] Suo G, Jiang S, Zhang J, Li J and He M 2014 Synthetic strategies and applications of GaN nanowires *Adv. Condens. Matter Phys.* **2014** 456163

[18] Alloing B and Zúñiga-Pérez J 2016 Metalorganic chemical vapor deposition of GaN nanowires: from catalyst-assisted to catalyst-free growth, and from self-assembled to selective-area growth *Mater. Sci. Semicond. Process.* **55** 51–8

[19] Bertness K A, Sanford N A and Davydov A V 2011 GaN nanowires grown by molecular beam epitaxy *IEEE J. Sel. Top. Quantum Electron.* **17** 847–58

[20] Chen L, Yin A, Im J-S, Nurmikko A V, Xu J M and Han J 2001 Fabrication of 50–100 nm patterned InGaN blue light emitting heterostructures *Phys. Status Solidi* a **188** 135–8

[21] Chen H-S, Yeh D-M, Lu Y-C, Chen C-Y, Huang C-F, Tang T-Y, Yang C C, Wu C-S and Chen C-D 2006 Strain relaxation and quantum confinement in InGaN/GaN nanoposts *Nanotechnology* **17** 1454–8

[22] Keller S *et al* 2006 Optical and structural properties of GaN nanopillar and nanostripe arrays with embedded InGaN/GaN multi-quantum wells *J. Appl. Phys.* **100** 054314

[23] Wang C-Y, Chen L-Y, Chen C-P, Cheng Y-W, Ke M-Y, Hsieh M-Y, Wu H-M, Peng L-H and Huang J 2008 GaN nanorod light emitting diode arrays with a nearly constant electroluminescent peak wavelength *Opt. Express* **16** 10549–56

[24] Ke M, Wang C, Chen L, Chen H, Chiang H, Cheng Y, Hsieh M, Chen C and Huang J 2009 Application of nanosphere lithography to LED surface texturing and to the fabrication of nanorod LED arrays *IEEE J. Sel. Top. Quantum Electron.* **15** 1242–9

[25] Tseng W-J, van Dorp D, Lieten R, Vereecken P, Langer R and Borghs G 2014 Impact of plasma-induced surface damage on the photoelectrochemical properties of GaN pillars fabricated by dry etching *J. Phys. Chem.* C **118** 11261–6

[26] Cho H, Khan F, Adesida I, Fang Z and Look D C 2008 Deep level characteristics in n-GaN with inductively coupled plasma damage *J. Phys. D: Appl. Phys.* **41** 155314

[27] Cao X, Cho H, Pearton S, Dang G, Zhang A, Ren F, Shul R, Zhang L, Hickman R and Van Hove J 1999 Depth and thermal stability of dry etch damage in GaN Schottky diodes *Appl. Phys. Lett.* **75** 232–4

[28] Cao X, Pearton S, Dang G, Zhang A, Ren F and Van Hove J 2000 GaN n-and p-type Schottky diodes: effect of dry etch damage *IEEE Trans. Electron Devices* **47** 1320–4

[29] Cao X, Piao H, LeBoeuf S, Li J, Lin J and Jiang H 2006 Effects of plasma treatment on the Ohmic characteristics of Ti/Al/Ti/ Au contacts to n-AlGaN *Appl. Phys. Lett.* **89** 082109

[30] Cao X, Zhang A, Dang G, Ren F, Pearton S, Van Hove J, Hickman R, Shul R and Zhang L 2000 Plasma damage in p-GaN *J. Electron. Mater.* **29** 256–61

[31] Keller S *et al* 2006 Optical and structural properties of GaN nanopillar and nanostripe arrays with embedded InGaN/GaN multi-quantum wells *J. Appl. Phys.* **100** 054314

[32] Pearton S J, Abernathy C R, Ren F, Lothian J R, Wisk P W and Katz A 1993 Dry and wet etching characteristics of InN, AlN, and GaN deposited by electron cyclotron resonance metalorganic molecular beam epitaxy *Journal of Vacuum Science & Technology* A **11** 1772–5

[33] Ping A, Schmitz A, Adesida I, Khan M A, Chen Q and Yang J 1997 Characterization of reactive ion etching-induced damage to n-GaN surfaces using schottky diodes *J. Electron. Mater.* **26** 266–71

[34] Ping A, Chen Q, Yang J, Khan M A and Adesida I 1998 The effects of reactive ion etching-induced damage on the characteristics of ohmic contacts to n-type GaN *J. Electron. Mater.* **27** 261–5

[35] Li Q, Westlake K R, Crawford M H, Lee S R, Koleske D D, Figiel J J, Cross K C, Fathololoumi S, Mi Z and Wang G T 2011 Optical performance of top-down fabricated InGaN/GaN nanorod light emitting diode arrays *Opt. Express* **19** 25528–34

[36] Wright J B, Li Q M, Luk T S, Brener I, Wang G T, Westlake K R and Lester L F 2011 Single-mode lasing from top-down fabricated gallium nitride nanowires *IEEE Photonic Society 24th Annual Meeting* pp 529–30

[37] Li Q, Wright J B, Chow W W, Luk T S, Brener I, Lester L F and Wang G T 2012 Single-mode GaN nanowire lasers *Opt. Express* **20** 17873–9

[38] Wang G T, Li Q, Wierer J, Figiel J, Wright J B, Luk T S and Brener I 2012 Top-down fabrication of GaN-based nanorod LEDs and lasers *SPIE OPTO* (SPIE) p 6

[39] Debnath R, Ha J-Y, Wen B, Paramanik D, Motayed A, King M R and Davydov A V 2014 Top-down fabrication of large-area GaN micro- and nanopillars *Journal of Vacuum Science & Technology* B **32** 021204

[40] Wang G T, Leung B, Tsai M C, Li C and Balakrihnan G 2017 Top-down etching of three-dimensional, high aspect ratio GaN nanostructures *11th Int. Symp. of Semiconductor Light Emitting Devices (Banff, Alberta, Canada)*

[41] Li Q, Figiel J J and Wang G T 2009 Dislocation density reduction in GaN by dislocation filtering through a self-assembled monolayer of silica microspheres *Appl. Phys. Lett.* **94** 231105

[42] Wang G T *et al* 2011 (Invited) III-Nitride nanowires: emerging materials for lighting and energy applications *ECS Trans.* **35** 3–11

[43] Westover T, Jones R, Huang J Y, Wang G, Lai E and Talin A A 2009 Photoluminescence, thermal transport, and breakdown in joule-heated GaN nanowires *Nano Lett.* **9** 257–63

[44] Xu H, Wright J B, Luk T-S, Figiel J J, Cross K, Lester L F, Balakrishnan G, Wang G T, Brener I and Li Q 2012 Single-mode lasing of GaN nanowire-pairs *Appl. Phys. Lett.* **101** 113106

[45] Munch U, Schneeberger N, Paul O, Baltes H and Doering E 1998 Thin film front protection of CMOS wafers against KOH *Micromachined Devices and Components IV* (International Society for Optics and Photonics) pp 124–33
[46] Álvarez C R B, Arriaga W C, Aranda M L and Jácome A T 2017 Anisotropic silicon etch to house CMOS compatible MEMS microstructures without planarization techniques *2017 14th Int. Conf. on Electrical Engineering, Computing Science and Automatic Control (CCE)* pp 1–4
[47] Alvarez H S, Silva A R, Espínola L C J, Vaz A R and Diniz J A 2021 NH4OH-B silicon texturing of periodic V-groove channels, upright, and inverted pyramids structures *IEEE J. Photovolt.* **11** 570–4
[48] Wierer J J Jr, Li Q, Koleske D D, Lee S R and Wang G T 2012 III-nitride core–shell nanowire arrayed solar cells *Nanotechnology* **23** 194007
[49] Talin A A *et al* 2010 Transport characterization in nanowires using an electrical nanoprobe *Semicond. Sci. Technol.* **25** 024015
[50] Bonard J M, Dean K A, Coll B F and Klinke C 2002 Field emission of individual carbon nanotubes in the scanning electron microscope *Phys. Rev. Lett.* **89** 197602
[51] Müller E W 1937 Beobachtungen über die Feldemission und die Kathodenzerstäubung an thoriertem Wolfram *Z. Phys.* **106** 132–40
[52] Telieps W and Bauer E 1985 An analytical reflection and emission UHV surface electron microscope *Ultramicroscopy* **17** 57–65
[53] Bauer E 2012 LEEM and UHV-PEEM: a retrospective *Ultramicroscopy* **119** 18–23
[54] Shul R J, McClellan G B, Pearton S J, Abernathy C R, Constantine C and Barratt C 1996 Comparison of dry etch techniques for GaN *Electron. Lett.* **32** 1408–9
[55] Sheu J K, Su Y K, Chi G C, Jou M J, Liu C C, Chang C M and Hung W C 1999 Inductively coupled plasma etching of GaN using Cl2/Ar and Cl2/N2 gases *J. Appl. Phys.* **85** 1970–4
[56] Harrison S E, Voss L F, Torres A M, Frye C D, Shao Q and Nikolić R J 2017 Ultradeep electron cyclotron resonance plasma etching of GaN *J. Vacuum Sci. Technol.* A **35** 061303
[57] Lothian J, Ren F and Pearton S 1992 Mask erosion during dry etching of deep features in III–V semiconductor structures *Semicond. Sci. Technol.* **7** 1199
[58] Ren F, Pearton S, Lothian J, Abernathy C and Hobson W 1992 Reduction of sidewall roughness during dry etching of SiO_2 *J. Vac. Sci. Technol.* B **10** 2407–11
[59] Lin C-F *et al* 2005 Self-assembled GaN:Mg inverted hexagonal pyramids formed through a photoelectrochemical wet-etching process *Electrochem. Solid-State Lett.* **8** C185
[60] Qi S L *et al* 2009 Study on the formation of dodecagonal pyramid on nitrogen polar GaN surface etched by Hot H3PO4 *Appl. Phys. Lett.* **95** 071114
[61] Jung Y *et al* 2011 Chemical etch characteristics of N-Face and Ga-Face GaN by phosphoric acid and potassium hydroxide solutions *J. Electrochem. Soc.* **159** H117
[62] Bharrat D, Hosalli A M, Van Den Broeck D M, Samberg J P, Bedair S M and El-Masry N A 2013 Gallium nitride nanowires by maskless Hot phosphoric wet etching *Appl. Phys. Lett.* **103** 082106
[63] Stocker D A, Schubert E F and Redwing J M 1998 Crystallographic wet chemical etching of GaN *Appl. Phys. Lett.* **73** 2654–6
[64] Mynbaeva M G 1999 Wet chemical etching of GaN in H3PO4 with AI Ions *Electrochem. Solid-State Lett.* **2** 404
[65] Han S-C *et al* 2010 Formation of hexagonal pyramids and pits on V-/VI-polar and III-/II-polar GaN/ZnO surfaces by wet etching *J. Electrochem. Soc.* **157** D60
[66] Reiner M, Reiss M, Brünig T, Knuuttila L, Pietschnig R and Ostermaier C 2015 Chemical understanding and utility of H3PO4 etching of group-III- nitrides *Phys. Status Solidi* B **252** 1121–6
[67] Leung B, Tsai M-C, Balakrishnan G, Li C, Brueck S R J, Figiel J J, Lu P and Wang G T Highly anisotropic crystallographic etching for fabrication of high-aspect ratio GaN nanostructures *Proc. 18th Int. Conf. on Metal Organic Vapor Phase Epitaxy (San DIego, CA)* p 45
[68] Sangwal K and Arora S K 1978 Etching of MgO crystals in acids: kinetics and mechanism of dissolution *J. Mater. Sci.* **13** 1977–85
[69] Jiang Y, Zhu G, Lin F, Zhang H, Jin C, Yuan J, Yang D and Zhang Z 2014 *In situ* study of oxidative etching of palladium nanocrystals by liquid cell electron microscopy *Nano Lett.* **14** 3761–5
[70] Hauwiller M R, Frechette L B, Jones M R, Ondry J C, Rotskoff G M, Geissler P and Alivisatos A P 2018 Unraveling kinetically-driven mechanisms of gold nanocrystal shape transformations using graphene liquid cell electron microscopy *Nano Lett.* **18** 5731–7
[71] Nijdam A J, Veenendaal E. v., Cuppen H M, Suchtelen J. v., Reed M L, Gardeniers J G E, Enckevort W. J. P. v., Vlieg E and Elwenspoek M 2001 Formation and stabilization of pyramidal etch hillocks on silicon {100} in anisotropic etchants: experiments and Monte Carlo simulation *J. Appl. Phys.* **89** 4113–23
[72] DeSalvo G C, Tseng W F and Comas J 1992 Etch rates and selectivities of citric acid/hydrogen peroxide on GaAs, Al0.3Ga0.7As, In0.2Ga0.8As, In0.53Ga0.47As, In0.52Al0.48As, and InP *J. Electrochem. Soc.* **139** 831–5
[73] Kern W 1978 Chemical etching of silicon, germanium, gallium arsenide, and gallium phosphide *RCA Rev.* **39** 278–94
[74] Ghandhi S K 1994 *VLSI Fabrication Principles: Silicon and Gallium Arsenide* (New York: Wiley)
[75] Li D, Sumiya M, Fuke S, Yang D, Que D, Suzuki Y and Fukuda Y 2001 Selective etching of GaN polar surface in potassium hydroxide solution studied by x-ray photoelectron spectroscopy *J. Appl. Phys.* **90** 4219–23
[76] Reiner M 2016 *Modification and Analysis of Group-13-Nitride Semiconductor Surfaces: Influence of Adsorbates on Device Characteristics and Processing* (Universität Kassel)
[77] Sangwal K 1987 *Etching of Crystals: Theory, Experiment, and Application* (Amsterdam, The Netherlands: North-Holland Physics Publishing)
[78] Qi S *et al* 2010 Fabrication of dodecagonal pyramid on nitrogen face GaN and its effect on the light extraction *Sci. China Technol. Sci.* **53** 769–71
[79] Lai Y-Y, Hsu S-C, Chang H-S, Wu Y S, Chen C-H, Chen L-Y and Cheng Y-J 2017 The study of wet etching on GaN surface by potassium hydroxide solution *Res. Chem. Intermediates* **43** 3563–72
[80] Fan Q 2016 A new method of calculating planar density: the position-duplication-number method *J. Appl. Crystallogr.* **49** 1454–8
[81] Dannecker K and Baringhaus J 2020 Fabrication of crystal plane oriented trenches in gallium nitride using SF6 + Ar dry etching and wet etching post-treatment *J. Vac. Sci. Technol.* A **38** 043204
[82] Choueib M, Ayari A, Vincent P, Bechelany M, Cornu D and Purcell S T 2009 Strong deviations from Fowler–Nordheim behavior for field emission from individual SiC nanowires due to restricted bulk carrier generation *Phys. Rev.* B **79** 075421
[83] Chung M S and Yoon B-G 2003 Analysis of the slope of the Fowler–Nordheim plot for field emission from n-type semiconductors *J. Vac. Sci. Technol.* B **21** 548–51
[84] Bhise A B, Late D J, Sathe B, More M A, Mulla I S, Pillai V K and Joag D S 2010 Fabrication of In-doped SnO_2 nanowire arrays and its field emission investigations *J. Exp. Nanosci.* **5** 527–35

[85] Carapezzi S, Castaldini A, Fabbri F, Rossi F, Negri M, Salviati G and Cavallini A 2016 Cold field electron emission of large-area arrays of SiC nanowires: photo-enhancement and saturation effects *J. Mater. Chem.* C **4** 8226–34
[86] Baskin L M, Lvov O I and Fursey G N 1971 General features of field emission from semiconductors *Phys. Status Solidi* b **47** 49–62
[87] Wang B, Zheng Z, Wu H and Zhu L 2014 Field emission properties and growth mechanism of In2O3 nanostructures *Nanoscale Res. Lett.* **9** 111
[88] Deb P, Westover T, Kim H, Fisher T and Sands T 2007 Field emission from GaN and (Al,Ga)N／GaN nanorod heterostructures *J. Vac. Sci. Technol.* B **25** L15–8
[89] Kanemaru S, Hirano T, Tanoue H and Itoh J 1997 Control of emission currents from silicon field emitter arrays using a built-in MOSFET *Appl. Surf. Sci.* **111** 218–23
[90] Talin A A, Wang G T, Lai E and Anderson R J 2008 Correlation of growth temperature, photoluminescence, and resistivity in GaN nanowires *Appl. Phys. Lett.* **92** 093105
[91] Calarco R, Marso M, Richter T, Aykanat A I, Meijers R, v.d. Hart A, Stoica T and Lüth H 2005 Size-dependent photoconductivity in MBE-Grown GaN−nanowires *Nano Lett.* **5** 981–4
[92] Li Q and Wang G T 2010 Spatial distribution of defect luminescence in GaN nanowires *Nano Lett.* **10** 1554–8
[93] Al-Tabbakh A A, More M A, Joag D S, Mulla I S and Pillai V K 2010 The Fowler–Nordheim plot behavior and mechanism of field electron emission from ZnO tetrapod structures *ACS Nano* **4** 5585–90
[94] Sim H S, Lau S P, Ang L K, You G F, Tanemura M, Yamaguchi K, Zamri M and Yusop M 2008 Field emission from a single carbon nanofiber at sub 100 nm gap *Appl. Phys. Lett.* **93** 023131
[95] Jensen K L 2019 A reformulated general thermal-field emission equation *J. Appl. Phys.* **126** 065302
[96] Nemanich R J, Baumann P K, Benjamin M C, Nam O H, Sowers A T, Ward B L, Ade H and Davis R F 1998 Electron emission properties of crystalline diamond and III-nitride surfaces *Appl. Surf. Sci.* **130–132** 694–703
[97] Nichols K E *et al* 2020 Demonstration of transport of a patterned electron beam produced by diamond pyramid cathode in an rf gun *Appl. Phys. Lett.* **116** 023502